Contribution of the tetrodotoxin-resistant voltage-gated sodium channel $Na_V1.9$ to sensory transmission and nociceptive behavior

Birgit T. Priest*, Beth A. Murphy*, Jill A. Lindia*, Carmen Diaz*, Catherine Abbadie*, Amy M. Ritter*, Paul Liberator*, Leslie M. Iyer†, Shera F. Kash†, Martin G. Kohler*, Gregory J. Kaczorowski*, D. Euan MacIntyre*, and William J. Martin*‡

*Merck Research Laboratories, P.O. Box 2000, Rahway, NJ 07065; and †Deltagen, Inc., San Carlos, CA 94070

Edited by William A. Catterall, University of Washington School of Medicine, Seattle, WA, and approved May 5, 2005 (received for review February 24, 2005)

The transmission of pain signals after injury or inflammation depends in part on increased excitability of primary sensory neurons. Nociceptive neurons express multiple subtypes of voltage-gated sodium channels (Na_V1s), each of which possesses unique features that may influence primary afferent excitability. Here, we examined the contribution of $Na_V1.9$ to nociceptive signaling by studying the electrophysiological and behavioral phenotypes of mice with a disruption of the *SCN11A* gene, which encodes $Na_V1.9$. Our results confirm that $Na_V1.9$ underlies the persistent tetrodotoxin-resistant current in small-diameter dorsal root ganglion neurons but suggest that this current contributes little to mechanical thermal responsiveness in the absence of injury or to mechanical hypersensitivity after nerve injury or inflammation. However, the expression of $Na_V1.9$ contributes to the persistent thermal hypersensitivity and spontaneous pain behavior after peripheral inflammation. These results suggest that inflammatory mediators modify the function of $Na_V1.9$ to maintain inflammation-induced hyperalgesia.

hyperalgesia | pain | mouse | inflammation | C-fibers

The generation and propagation of action potentials in sensory neurons depends on the activity of voltage-gated sodium channels (Na_V1s). The differential expression of Na_V1 subtypes in distinct classes of sensory neurons, combined with their unique biophysical properties, suggest specific roles for each subtype in sensory transmission. Sodium channels in sensory neurons can be classified pharmacologically as sensitive to block by low nanomolar concentrations of tetrodotoxin (TTX) or resistant to >1 μM TTX (1, 2).

The contribution of TTX-resistant Na_V1 channel subtypes to the transmission of pain signals is an important area of focus: TTX-resistant current carries the majority of charge during action potentials in nociceptive neurons (3), and this current is dynamically regulated in response to injury (4, 5). $Na_V1.8$, expressed primarily in C-fibers (6), underlies a TTX-resistant current with a high threshold for activation and steady-state inactivation and slow kinetics (7). Comparisons between dorsal root ganglion (DRG) neurons from WT and $Na_V1.8$ null mutant ($-/-$) mice suggest that $Na_V1.8$ contributes the majority of the inward current flowing during action potentials in small-diameter neurons (8). Antisense oligonucleotides directed against $Na_V1.8$ implicate this channel in both neuropathic (9) and inflammatory (10) pain conditions in rats, although $Na_V1.8-/-$ mice displayed only a mild phenotype (7, 11).

The functional role of $Na_V1.9$, another subtype selectively expressed in nociceptors (12), remains poorly defined. The primary sequence of $Na_V1.9$ predicts that this subtype conducts sodium currents resistant to TTX (13). Indeed, a second TTX-resistant current is present in DRG neurons from $Na_V1.8$ knockout mice (14). This current has been referred to as the persistent, TTX-resistant current because of its negative threshold for activation and depolarized midpoint of inactivation, resulting in a significant window current (14). Activation and inactivation kinetics of this current are slow, and the current shows prominent ultraslow inactivation. The overlapping expression of $Na_V1.9$ and the persistent TTX-resistant current in myenteric neurons (15) and DRG neurons that bind isolectin IB4 (16) supports the notion that $Na_V1.9$ carries the persistent TTX-resistant current.

The failure to express $Na_V1.9$ in heterologous systems has prevented a complete characterization of this subtype. Moreover, little is known about the extent to which $Na_V1.9$ contributes to nociceptive signaling. Knockdown of $Na_V1.9$ through the use of antisense oligodeoxynucleotides suggests that $Na_V1.9$ is not involved in acute nociception or the maintenance of nerve injury-induced hyperalgesia (17). A direct role of $Na_V1.9$ in inflammatory hyperalgesia has not been investigated, although there is evidence that a TTX-resistant current not carried by $Na_V1.8$ is modified by inflammatory mediators (18).

In this study, we used null mutant mice to demonstrate that $Na_V1.9$ is the molecular correlate of the persistent current and examine its role in nociceptive signaling.

Materials and Methods

All procedures involving animals were carried out in accordance with the guidelines issued by the National Institutes of Health and approved by the Merck Research Laboratories-Rahway Institutional Animal Care and Use Committee.

Materials. TaqMan primer and probe sequences for *SCN1A* (Mm00450580_m1), *SCN3A* (Mm00658167_m1), *SCN8A* (Mm00488110_m1), *SCN9A* (Mm00450762_s1), *SCN10A* (Mm00501467_m1), and *SCN11A* (Mm00449377_m1) were purchased from Applied Biosystems. TaqMan primer and probe sequences for *SCN1B* and *SCN3B* were custom-ordered from Applied Biosystems as follows (reverse primer, TaqMan probe, forward primer): *SCN1B*, 5′-ACAGTAGTGGGCAGGAGGTT-3′, FAM-CTGGGCCTCATCTCC, 5′-AGGTCCAGCCGGAG-GAA-3′; and *SCN3B*, 5′-CTTCCGGACTCTATCAGAACTC-CTA-3′, FAM-ACCTTGCCTGAACTGAAG, 5′-TGAGGTT-TAGTCCATGGAGAGATGT-3′.

Generation of *SCN11A*$-/-$ Mice. *SCN11A*$-/-$ mice were obtained from Deltagen (San Carlos, CA). A 6.93-kb internal ribosome entry site (IRES)-lacZ reporter and neomycin resistance cassette (IRES-lacZ-neo) was subcloned into a 3.4-kb fragment isolated from a mouse genomic phage library, such that 174 bp (base pairs 379–552) of the coding region were replaced by IRES-LacZ-neo. The IRES-lacZ-neo cassette was flanked by 1.8 and 1.6 kb of mouse genomic DNA at its 5′ and 3′ aspects, respectively. The linearized

This paper was submitted directly (Track II) to the PNAS office.

Abbreviations: DRG, dorsal root ganglion; Na_V1, voltage-gated sodium channel; TTX, tetrodotoxin; IRES, internal ribosome entry site; CFA, complete Freund's adjuvant; PGE_2, prostaglandin E2.

‡To whom correspondence should be addressed. E-mail: william_martin@merck.com.

www.pnas.org/cgi/doi/10.1073/pnas.0501549102

targeting vector was electroporated into 129/OlaHsd mouse ES cells. ES cells were selected for G418 resistance, and colonies carrying the homologously integrated targeting construct were identified by PCR amplification by using a 5′ neo-specific primer (5′-GGGATCTTGGCCATGGTAAGCTGAT-3′) paired with a primer located outside the targeting homology arms on the 5′ side (GS1: 5′-GAGTCATTGCCTGGGTGCATGGTCT-3′). The homologous recombination event was confirmed on the 3′ side by using a 3′ neospecific primer (5′-ACGTACTCGGATGGAAGCCGGTCTT-3′) paired with a primer located outside the targeting homology arm on the 3′ side (GS2: 5′-GCCTCACTAGAGCTGGCATTATAAG-3′). ES cell colonies that gave rise to the correct size of PCR product were confirmed by Southern blot analysis with a probe adjacent to the 5′ region of homology. The presence of a single neo cassette was confirmed by Southern blot analysis with a neo gene fragment as a probe. Male chimeric mice were generated by injection of the targeted ES cells into C57BL/6J blastocysts. Chimeric mice were bred with C57BL/6J mice to produce F_1 heterozygotes. Germ-line transmission was confirmed by PCR analysis. After confirmation of the targeting event in animals, subsequent genotyping tracked transmission of the targeting construct. F_1 heterozygous males and females were mated to produce F_2 WT, heterozygous, and homozygous null mutant animals. Mice were backcrossed with C57BL/6J mice, and all phenotypic analysis was performed in a hybrid C57BL/6J/129 background (75%/25%, respectively). Mice were maintained in a temperature-controlled (23°C) barrier facility with a 12-h light/dark cycle and had ad libitum access to water and regular rodent chow.

Real-Time Quantitative PCR. Real-time quantitative PCR was used to compare mRNA expression of $Na_V1.1$–1.3, $Na_V1.6$–1.8, *SCN1B* (β1), and *SCN3B* (β3) in eight DRGs from four WT and four $Na_V1.9-/-$ mice. Total RNA was prepared by using TRIzol (Life Technologies, Gaithersburg, MD) followed by RNeasy (Qiagen, Hilden Germany) and treated with RNase-free DNase I. cDNA was synthesized by priming with random hexamer oligos using the SuperScript first-strand synthesis system for RT-PCR (Invitrogen). Real-time PCR was performed on an Applied Biosystems Prism 7700 sequence detection system. Forward and reverse amplification primers were included at a final concentration of 900 nM, and the oligonucleotide probe concentration was 200 nM. Each PCR was performed in triplicate in a final volume of 50 μl by using cDNA prepared from 10 ng of RNA as template. The TaqMan Universal PCR Master Mix containing AmpliTaq Gold DNA Polymerase (Applied Biosystems) and dNTPs were used according to the manufacturer's instructions for a singleplex real-time PCR.

Analysis of Relative Gene Expression. A preparation of cDNA from a pool of 50 mouse DRGs (Charles River Laboratories) was used to construct eight-point standard curves for amplicons derived from each of the following genes: $Na_V1.1$–1.3, $Na_V1.6$–1.8, *SCN1B*, *SCN3B* (0.3125–40 ng of cDNA), and 18S rRNA (0.0078–1 ng of cDNA). RNA equivalents in each biological sample were calculated from the respective standard curves and normalized to 18S rRNA.

DRG Preparation. DRG was dissected from mice that were overdosed with Nembutal (100 mg/kg, i.p.). Ganglia from all levels were washed once with F14 growth media, consisting of 10% F14, 10% horse serum, 1% Pen/strep (5,000 units/500 μg), and 0.12% $NaHCO_3$. Ganglia were then incubated in F14 containing 0.125% collagenase (type I) for 30 min at 37°C, followed by 0.05% trypsin for 8 min at 37°C. Ganglia were washed once with F14 and triturated with a fire-polished pipette to obtain a single cell suspension, which was plated onto poly-D-lysine-coated glass coverslips. All recordings were made within 2–30 h of ganglia isolation.

Electrophysiology. Sodium currents were examined by whole-cell voltage clamp by using an EPC-9 amplifier and PULSE software (HEKA Electronics, Lamprecht, Germany). For voltage–clamp recordings, the bath solution contained 40 mM NaCl, 30 mM tetraethylammonium (TEA)-C1, 70 mM *N*-methyl-D-glucamine Cl, 2.7 mM $CaCl_2$, 0.5 mM $MgCl_2$, 0.1 mM $CdCl_2$, 10 mM *N*-methyl-D-glucamine-Hepes, plus 300 nM TTX, pH 7.4, and the internal solution contained 145 mM CsF, 5 mM NaCl, 1 mM EGTA (tetra Cs salt), 10 mM Cs Hepes, pH 7.4. We did not correct for liquid junction potentials. Voltage errors were minimized by series resistance compensation (75–85%), and the capacitance artifact was canceled by using the amplifier's built-in circuitry. Data were acquired at 50 kHz and filtered at 8–10 kHz. For current clamp recordings, the bath solution contained 140 mM NaCl, 3 mM KCl, 1 mM $CaCl_2$, 1 mM $MgCl_2$, 10 mM Na-Hepes, pH 7.4, and the internal solution contained either 110 mM K aspartate, 20 mM KF, 5 mM NaCl, 2 mM $MgCl_2$, 0.5 mM EGTA, 5 mM MgATP, 0.5 mM Li_2GTP, and 10 mM Na-Hepes, pH 7.4 or 130 mM K aspartate, 5 mM NaCl, 2 mM $MgCl_2$, 0.5 mM EGTA, 5 mM MgATP, 0.5 mM Li_2GTP, and 10 mM Na-Hepes, pH 7.4. No difference were noted between the two intracellular solutions.

Skin-Nerve Preparation. To measure C-fiber thresholds and compound action potentials, mice were overdosed with Nembutal (100 mg/kg i.p.) and perfused through the heart with ice-cold synthetic interstitial fluid (composition: 108 mM NaCl, 3.5 mM KCl, 1.5 mM $CaCl_2$, 0.7 mM $MgSO_4$, 26 mM $NaHCO_3$, 1.7 mM NaH_2PO_4, 5.5 mM D-glucose, 9.6 mM NaGluconate, and 7.6 mM sucrose). The fur along the back was clipped closely, and the back skin along with four to five dorsal cutaneous nerves was removed (19). The skin was placed epidermal-side up atop a mesh platform, with the surface of the skin at the air/fluid interface in a recirculating bath bubbled with 95% O_2/5% CO_2 at 30°C. The cut end of one nerve was placed in an oil-filled chamber and manually dissociated into fine filaments for extracellular recording. The skin was searched with a blunt probe, and mechanically responsive units were characterized by determining mechanical threshold with hand-held von Frey hairs, and by applying a heat ramp of 1°C/s from 37°C to 50°C directly to the surface of the skin by using a liquid-cooled resistive thermode. The receptive field was stimulated electrically with a concentric needle electrode to determine latency and verify C-fiber conduction velocity. Data were digitized and recorded for post hoc analysis by using SPIKE2 software (Cambridge Electronic Design, Cambridge, U.K.). For compound action potential recording, one end of the dorsal cutaneous nerve was placed in an oil-filled chamber, desheathed, and draped over a bipolar recording electrode. The other end was stimulated with a suction electrode (0.5-ms duration pulse at 0.5, 1, 5, or 10 Hz). A total of 19 C-fibers were characterized in WT mice and 18 were characterized in $Na_V1.9-/-$ mice. Compound action potentials were recorded from six dorsal cutaneous nerves from three WT mice, and four nerves were recorded from three $Na_V1.9-/-$ mice.

Behavioral Models. Thermal sensitivity was assessed by measuring paw withdrawal latencies to a radiant heat stimulus (20) or by placing the mice on a hotplate with the temperature sequentially set to 52.5°C, 55.5°C, and 58.5°C (cut-off set at 20 s). The latency to hind-paw licking or jumping was recorded. Mechanical sensitivity was determined with calibrated von Frey filaments (Stoelting) using the up-and-down paradigm (21). Motor coordination was assessed by measuring the ability to walk on an accelerating rotorod. Mice were placed on the rotorod at a starting speed of 2 rpm and an acceleration rate of 0.1 rpm/s. The procedure was repeated until the animal was able to walk continuously for 2 min. Total walking time and the number of trials required to reach the 2-min criterion were recorded. For the nerve injury model, mice ($n = 16$ per group) were anesthetized with a mixture of ketamine (50 mg/kg, i.m., Pfizer Animal Health, Exton, PA) and medetomidine (1 mg/kg, i.m., Pfizer Animal Health). The sciatic nerve was exposed just below the hip bone, and ⅓ to ½ of the sciatic nerve was tightly

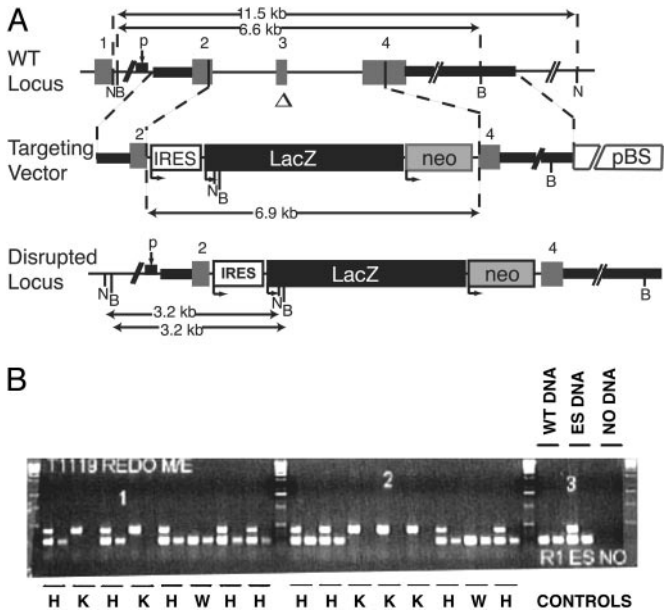

Fig. 1. Disruption of *SCN11A* ($Na_V1.9$) in mouse ES cells and generation of $Na_V1.9-/-$ mice. (*A*) Structure of WT and mutant *SCN11A* loci. Thick solid lines denote genomic sequence within the targeting construct. A 174-bp region (Δ) of the *SCN11A* coding sequence was replaced by a 6.9-kb IRES-LacZ reporter and neomycin resistance cassette (IRES-LacZ-neo). The numbers designate the exons. B and N indicate restriction sites for BamHI and NcoI, respectively. Two overlapping oligonucleotide probes used to hybridize Southern blots are indicated by p. pBS denotes Bluescript vector sequence. (*B*) The first reaction multiplex for each sample includes three primers (neo- and gene-specific) and simultaneously detects the endogenous (233 bp) and targeted (424 bp) alleles. The second reaction includes only gene-specific primers and detects only the endogenous allele. Reactions using either no DNA (−) or DNA obtained from F_2 mice or ES cells are shown. W, WT; H, heterozygote; K, homozygous null mutant.

ligated with 6-0 silk suture thread (22). Sensitivity to mechanical stimulation was tested before and up to 28 d after nerve injury by using von Frey filaments. For the formalin test, mice were administered 10 μl of 2% formalin into the plantar surface of the left hind paw. The time spent licking or lifting the injected paw during 2-min intervals was recorded every 5 min for 60 min postinjection. For the carrageenan model, mice received a 20-μl intraplantar injection of carrageenan (0.6 mg/20 μl) into the left hind paw. Thermal sensitivity was assessed before and up to 24 h after injection. For the complete Freund's adjuvant (CFA) model, mice received a unilateral 30-μl injection of CFA (0.5 mg/30 μl) into the plantar surface of the left hind paw. Sensitivity to thermal and mechanical stimulation was assessed before and up to 2 wk after CFA administration. To study prostaglandin E2 (PGE_2)-induced hyperalgesia, +/+ mice ($n = 8$), +/− mice ($n = 8$), and −/− mice ($n = 8$) received intaplantar PGE_2 (0.01 mg/20 μl) injected into the left hind paw. Latency for paw withdrawal from a radiant heat source was assessed at 0.25, 0.5, 1, 2, 3, and 24 h postinjection. Carrageenan, CFA, and PGE_2 were purchased from Sigma and were dissolved in sterile saline.

Results

Disruption of *SCN11A*. To generate $Na_V1.9$ mutant mice, a section of the *SCN11A* gene encoding $Na_V1.9$ was replaced by homologous recombination in ES cells with a cassette containing the neomycin resistance and β-galactosidase genes (Fig. 1*A*). The resulting deletion of 174 bp, starting in exon 2 and ending in exon 4 of the coding sequence of *SCN11A* and corresponding to the first and second membrane-spanning segments in domain I of $Na_V1.9$, renders the protein nonfunctional. Gene targeting of neomycin-resistant ES cells was examined by 5′ and 3′ PCR using gene-specific primers paired with primers recognizing the neomycin resistance gene and confirmed by Southern blot analysis. Mice were genotyped by PCR using genomic DNA from tail biopsies (Fig. 1*B*).

Table 1. Relative expression of Na_V1 mRNAs in DRGs collected from WT and $Na_V1.9-/-$ mice

Na_V subunit	RNA equivalents		Relative expression
	WT	$Na_V1.9-/-$	$Na_V1.9-/-$/WT
$Na_V1.1$	0.52 ± 0.09	0.94 ± 0.09	1.79 ± 0.36
$Na_V1.2$	0.54 ± 0.08	0.72 ± 0.06	1.34 ± 0.23
$Na_V1.3$	0.53 ± 0.05	0.87 ± 0.02	1.65 ± 0.15
$Na_V1.6$	0.72 ± 0.11	0.72 ± 0.08	1.00 ± 0.18
$Na_V1.7$	0.47 ± 0.07	0.86 ± 0.13	1.82 ± 0.38
$Na_V1.8$	1.11 ± 0.14	1.64 ± 0.22	1.48 ± 0.27
$Na_V1.9$	1.69 ± 0.53	0.18 ± 0.02	0.11 ± 0.04
β1 (*SCN1B*)	0.65 ± 0.15	0.74 ± 0.20	1.14 ± 0.41
β3 (*SCN3B*)	0.53 ± 0.09	0.94 ± 0.22	1.77 ± 0.50

$Na_V1.9-/-$ mice were not significantly different from age- and gender-matched WT littermates with respect to length, weight, blood chemistry, fertility, and lifespan. Necropsy and histology showed no differences between genotypes.

Because changes in expression levels of other sodium channel subtypes may mask the phenotypic consequences of $Na_V1.9$ deletion, real-time quantitative PCR was used to compare mRNA expression levels of $Na_V1.1$–1.3, $Na_V1.6$–1.8, *SCN1B* (β1), and *SCN3B* (β3) in DRGs from WT and $Na_V1.9-/-$ mice. Only marginal increases (<2-fold) in mRNA expression were detected for each of the target genes (Table 1).

$Na_V1.9$ Carries the Persistent TTX-Resistant Current in DRG Neurons. In whole-cell voltage-clamp recordings from acutely dissociated DRG neurons, using fluoride as the major intracellular anion, two TTX-resistant currents could be distinguished based on their voltage dependence of activation and their time course of activation and inactivation. Similar to previous reports (14), we observed a TTX-resistant current that activated during pulses to voltages as

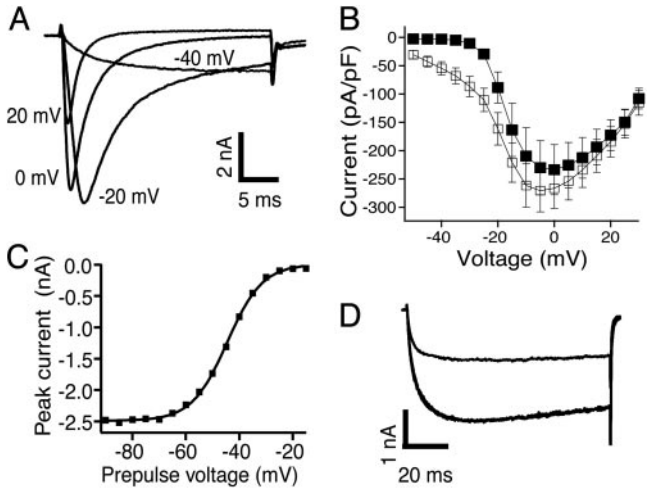

Fig. 2. Properties of the persistent sodium current in small-diameter DRG neurons. (*A*) TTX-resistant sodium current elicited by steps to −40, −20, 0, and +20 mV from a holding potential of −90 mV. (*B*) Average amplitude of the TTX-resistant sodium current as a function of test pulse voltage in WT (□, $n = 26$) and $Na_V1.9-/-$ (■, $n = 18$) neurons. (*C*) Peak current elicited by pulses to −40 mV as a function of membrane potential during a 0.5-s prepulse. A fit of the data to the Boltzman equation yielded $V_h = -44.6$ mV and $k = 6.6$ mV. (*D*) Current elicited by pulses to −40 mV in control (black line) and 500 μM lidocaine (gray line).

Table 2. Action potential properties of DRG neurons from WT $Na_V1.9-/-$ mice

Genotype	Cap, pF	RMP, mV	IR, GΩ	Amplitude, mV	Duration, ms	*n*	AHP, mV	Threshold, mV	Rheobase, pA	No. of APs at × rheobase		*n*
										x = 2	*x* = 3	
WT	16.9 ± 1.2	−47.8 ± 1.7	1.2 ± 0.2	49.3 ± 1.3	5.7 ± 0.4	24	−18.6 ± 1.4	−26.1 ± 1.5	33.2 ± 7.5	2.5 ± 0.4	3.3 ± 0.5	24
$Na_V1.9-/-$	15.0 ± 1.2	−48.6 ± 2.4	1.1 ± 0.2	50.4 ± 1.9	6.7 ± 0.5	23	−16.2 ± 1.3	−22.6 ± 2.6	48.3 ± 13.1	1.7 ± 0.3	2.8 ± 0.5	23

Cap, capacitance; RMP, resting membrane potential; IR, input resistance; AHP, after hyperpolarization; AP, action potential.

negative as −50 mV (Fig. 2 *A* and *B*). At −40 mV, the persistent current was characterized by a slow activation time constant of 5.0 ± 0.3 ms ($n = 38$), no discernible inactivation during a 30-ms test pulse, and rapid deactivation (Fig. 2*A*). A 1-s pulse to −40 mV revealed an inactivation constant of 0.5 s (data not shown). The deactivation time constant at −100 mV was <1 ms, unlike a rarely seen potassium current with a deactivation time constant of 3.3 ± 0.3 ms ($n = 3$), similar to the previously described sustained current I_{Ki} (23). A trait of the persistent TTX-resistant current was a slow run-up lasting several minutes after the whole-cell configuration was obtained.

Because the other TTX-resistant sodium current, carried by $Na_V1.8$, had a significantly more positive voltage range of activation, steady-state inactivation of the persistent TTX-resistant current could be examined in isolation by using a test pulse to −40 mV (Fig. 2*C*). For 0.5-s conditioning pulses, the midpoint of steady-state inactivation was −45.1 ± 2.9 ms ($n = 11$). Partial replacement of extracellular Na^+ with *N*-methyl-D-glucamine caused the expected decrease in the amplitude of the current activated by pulses to −40 mV, suggesting that this current was indeed carried by Na^+ ions. As expected based on the primary sequence of $Na_V1.9$, the persistent current was insensitive to 300 nM TTX and 100 nM saxitoxin ($n = 6$; data not shown). The persistent current was, however, blocked by the local anesthetic lidocaine. In two experiments, 500 μM lidocaine blocked 52% and 55% of the current activated during 100-ms voltage steps to −40 mV from a holding potential of −100 mV (Fig. 2*D*). This sensitivity to lidocaine was similar to that reported for the resting-state block of the TTX-resistant current in rat DRGs (24) and of several recombinant Na_V1 channel subtypes (25, 26), suggesting that the pharmacology of $Na_V1.9$ may be similar to that of other Na_V1 subtypes.

A TTX-resistant persistent sodium current with the characteristics described in Fig. 2 was observed in 39 of 42 small-diameter (<28 μm) DRG neurons from WT mice but was not detected in any of 18 neurons from $Na_V1.9-/-$ mice. Fig. 2*B* shows average current–voltage relationships, normalized by cell capacitance, for the TTX-resistant sodium current in WT and $Na_V1.9$ null neurons. In contrast to WT neurons, $Na_V1.9$ null neurons display no measurable current at test potentials more negative than −30 mV. WT and $Na_V1.9$ null neurons did not differ in size based on cell capacitance measurements (WT, 16.1 ± 0.8 pF; $Na_V1.9$ null, 15.8 ± 1.1 pF, $P = 0.84$), and recordings were carried out at the same holding potentials and for sufficient time to account for any current run-up.

$Na_V1.9$ Does Not Influence Action Potential Properties in DRG Neurons. To assess the contribution of $Na_V1.9$ to resting membrane potential and action potential characteristics, we compared current–clamp recordings, performed with near-physiological concentrations of Na^+ and K^+, in 24 small-diameter DRG neurons from three WT mice and 23 neurons from four $Na_V1.9-/-$ mice. Results are summarized in Table 2. Capacitance measurements indicated no significant difference in the size of WT and $Na_V1.9-/-$ neurons chosen for this study ($P = 0.29$). Neurons from WT and $Na_V1.9-/-$ animals did not differ significantly with regard to resting membrane potential and input resistance ($P = 0.79$ and $P = 0.62$, respectively). Spontaneous action potentials were observed in one WT and three $Na_V1.9-/-$ neurons; current injection elicited action potentials in all other neurons tested. Neurons from WT and $Na_V1.9-/-$ animals exhibited comparable action potential threshold ($P = 0.24$), amplitude ($P = 0.61$), duration ($P = 0.12$), and after hyperpolarization ($P = 0.21$). Whereas rheobase, defined as the current required to elicit action potentials, was somewhat greater for neurons from $Na_V1.9-/-$ animals and the number of action potentials elicited at two times rheobase was smaller, these differences were not statistically significant ($P = 0.31$ and $P = 0.09$, respectively).

$Na_V1.9$ Does Not Contribute to Peripheral Nerve Stimulus-Response Properties. To test whether $Na_V1.9$ participates in the recruitment and activation of A- and C-fibers, we examined the compound action potential waves of intact cutaneous nerves in response to repetitive whole nerve stimulation. Table 3 shows the data, presented as the ratio of the amplitude of the 20th pulse as compared with the first pulse, for the A- and C-wave components. Increasing stimulus frequency had no effect on the A wave, and we detected no difference between WT and $Na_V1.9-/-$ mice. Consistent with a lack of effect on resting membrane potential or action potential properties in dissociated neurons, we found that the amplitude of the C wave decreased as a function of stimulation frequency to the same extent in both genotypes (Table 3).

Next, we characterized the mechanical and thermal thresholds of C-fibers from WT and $Na_V1.9-/-$ mice. Dissection of a flap of skin from the back of the mouse complete with attached cutaneous nerves permits the *in vitro* measurement of C-fiber responses, evoked by mechanical or thermal stimulation of the receptive field. Mechanical thresholds, determined by stimulating the skin with an ascending series of von Frey filaments, were comparable in WT and $Na_V1.9-/-$ mice (0.79 ± 1.2 g for +/+ vs. 0.51 ± 0.63 g for −/−, $P > 0.05$ Student's *t* test; Fig. 3*A Left*). Thermal thresholds, determined by using a contact thermode and heat ramp stimuli, were also comparable between genotypes (44.3 ± 3.9°C for +/+ vs. 45.8 ± 3.9°C for −/−, $P > 0.05$ Student's *t* test; Fig. 3*A Right*).

$Na_V1.9$ Selectively Reduces the Duration of Inflammatory Pain Behavior. To examine the contribution of $Na_V1.9$ to pain signaling, we compared the $Na_V1.9-/-$ mice and their WT littermates in a range of pain models.

Table 3. Compound action potentials in WT and $Na_V1.9-/-$ mice

Genotype	A-wave				C-wave			
	0.5 Hz	1 Hz	5 Hz	10 Hz	0.5 Hz	1 Hz	5 Hz	10 Hz
WT	101 ± 3%	101 ± 3%	100 ± 4%	97 ± 5%	93 ± 6%	89 ± 10%	72 ± 20%	63 ± 23%
$Na_V1.9-/-$	100 ± 3%	101 ± 2%	100 ± 3%	101 ± 3%	103 ± 3%	94 ± 5%	81 ± 21%	65 ± 14%

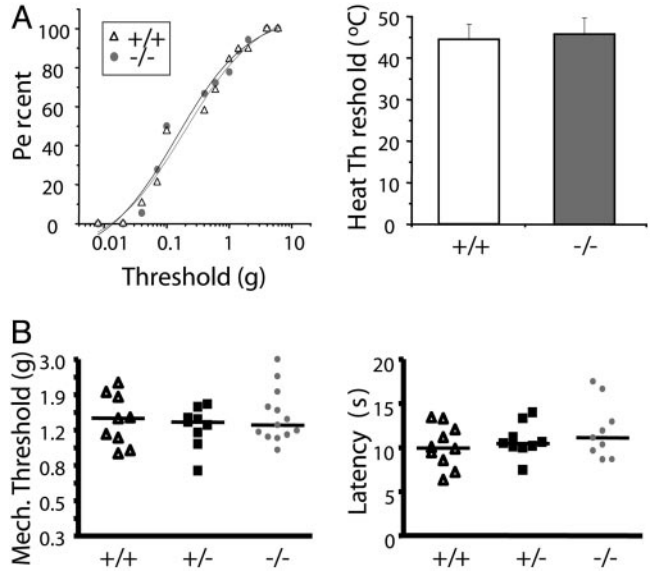

Fig. 3. Mechanical and thermal stimulus-induced primary afferent and behavioral response thresholds in $Na_V1.9-/-$ mice. (*A*) *In vitro* measurement of C-fiber responses, evoked by mechanical (*Left*) and thermal (*Right*) stimulation of the skin. (*B*) Behavioral response thresholds of WT (△), heterozygous (■), and $Na_V1.9-/-$ mice (gray circles) to mechanical stimulation (*Left*, n = 9–13) and radiant heating of the plantar hind paw (*Right*, n = 9–13).

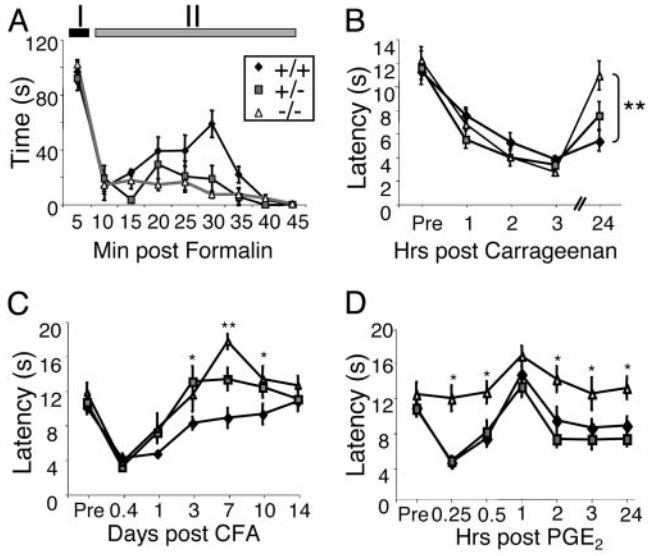

Fig. 4. Inflammatory hyperalgesia in $Na_V1.9-/-$ mice. (*A*) Time course of spontaneous behavioral responses to intraplantar injection of formalin (n = 11, $Na_V1.9+/+$; n = 7, $Na_V1.9+/-$; n = 15, $Na_V1.9-/-$). (*B–D*) Withdrawal latencies in response to radiant heating of the paw after injection with inflammatory mediators. (*B*) Duration of carrageenan-induced thermal hyperalgesia in $Na_V1.9-/-$ mice (n = 8) was shorter than in WT (n = 7) and $Na_V1.9+/-$ mice (n = 8). Unpaired t test; **, $P < 0.01$. (*C*) CFA-induced thermal hyperalgesia was significantly less in $Na_V1.9-/-$ (n = 9) and $Na_V1.9+/-$ mice (n = 9), compared with WT mice (n = 10). Repeated measures ANOVA followed by Fisher's probable least-squares difference; *, $P < 0.05$; **, $P < 0.01$ (post hoc analyses only). (*D*) Unlike WT mice (n = 8) and $Na_V1.9+/-$ mice (n = 8), $Na_V1.9-/-$ mice (n = 8) failed to develop significant PGE_2-induced thermal hyperalgesia. Repeated measures ANOVA followed by Fisher's probable least-squares difference; *, $P < 0.05$ for $Na_V1.9-/-$, compared with WT mice.

In agreement with the lack of effect on C-fiber thresholds, we found no differences between genotypes in acute sensitivity to mechanical stimulation or to noxious thermal stimulation, applied through a radiant heat source (Fig. 3*B*). Behavioral responses on a 52°C, 55°C, or 58°C hotplate were comparable among the three genotypes (data not shown). Motor coordination in $Na_V1.9$ WT mice (n = 13) and $-/-$ mice (n = 11) was normal as judged by the number of trials required (five) for the mice to walk continuously for 2 min on a rotating cylinder and by the total walking time (623 ± 24 s and 640 ± 40 s, respectively).

Partial ligation of the sciatic nerve induces a chronic pain state that develops within 1–2 days after the injury and persists for several weeks. A characteristic of this chronic pain state is the development of mechanical hypersensitivity to a previously innocuous stimulus (allodynia) in the affected hind paw. WT, heterozygous, and $Na_V1.9-/-$ mice were examined for their sensitivity to mechanical stimuli before and on various days after sciatic nerve injury. All animals developed profound mechanical allodynia that persisted for the length of the study (4 weeks), and we observed no differences among the genotypes (P = 0.45).

In contrast to the lack of effect in the neuropathic pain model, heterozygous and homozygous $Na_V1.9-/-$ mice presented with prominent differences in pain responses to inflammatory stimuli, compared with their WT littermates. In the formalin test, intraplantar injection of dilute (2%) formalin produced two phases of spontaneous pain behavior as evidenced by flinching and/or licking of the injected hind paw (Fig. 4*A*). Pain behavior during the first phase of the test (I: 0–5 min), did not differ between genotypes; however, during the late phase (II: 10–45 min) heterozygous and homozygous $Na_V1.9-/-$ mice displayed significantly reduced (by ≈50%) pain behavior (one-way ANOVA, $P < 0.0001$; followed by Bonferroni's post hoc, $P < 0.001$).

Based on these results, we tested whether $Na_V1.9$ contributes to stimulus-evoked behavioral responses in the setting of inflammation. Intraplantar injection of carrageenan induced significant ($F_{4,34}$ = 13.6; $P < 0.0001$) thermal hyperalgesia in WT and heterozygous mice ($F_{4,39}$ = 11.7; $P < 0.0001$) at each time point tested (1, 2, 3, and 24 h postinjection; Dunnett's post hoc, $P < 0.05$; Fig. 4*B*). Homozygous $Na_V1.9-/-$ mice also developed thermal hyperalgesia ($F_{4,39}$ = 16.4; $P < 0.0001$); however, in contrast to WT and heterozygous mice, $Na_V1.9-/-$ mice failed to exhibit thermal hyperalgesia 24 h postinjection of carrageenan, at which time thermal hyperalgesia was still present in WT mice (−5.9 + 0.9-s difference from baseline) and significantly different from $Na_V1.9-/-$ mice (−1.3 + 0.9 s; $P < 0.01$, unpaired t test: Fig. 4*B*). Similarly, intraplantar injection of CFA significantly decreased nociceptive thresholds in all genotypes of mice ($F_{2,25}$ = 11.8; P = 0.0002), but the time course of the thermal hyperalgesia differed significantly ($F_{12,150}$ = 2.4; P = 0.009; Fig. 4*C*). Compared with baseline responses, thermal hyperalgesia was observed in heterozygous and homozygous $Na_V1.9-/-$ mice only at 6 and 24 h after CFA injection and only reached statistical significance at the 6-h time point ($P < 0.01$, Dunn's multiple comparison). By contrast, thermal hyperalgesia persisted in WT littermates until 3 days after CFA injection. Development and progression of mechanical allodynia was comparable in all genotypes (data not shown).

Because inflammatory mediators, including PGE_2, modulate TTX-resistant sodium current (27), we tested the ability of PGE_2 to induce thermal hyperalgesia in WT and $Na_V1.9$ mutant mice. We found that thermal hyperalgesia developed in WT and heterozygous mice ($F_{2,6}$ = 17.1; $P < 0.001$) and that this behavioral hypersensitivity was significantly greater (Fisher's protected least significant difference; $P < 0.001$) than that observed in $Na_V1.9-/-$ mice, in which hyperalgesia was essentially absent (Fig. 4*D*).

Discussion

Here, we examined the contribution of $Na_V1.9$ to nociceptive signaling by studying the electrophysiological and behavioral phenotypes of mice with a disruption of the *SCN11A* gene encoding $Na_V1.9$. Our results confirm that $Na_V1.9$ underlies the persistent

TTX-resistant current in DRG neurons, but suggest that this current contributes little to mechanical or thermal responsiveness in the absence of injury or to mechanical hypersensitivity after nerve injury or inflammation. *In vitro* experiments, using a skin-nerve preparation, indicated that C-fiber mechanical and thermal thresholds did not differ between $Na_V1.9-/-$ mice and their WT littermates. Consistent with this finding, acute behavioral mechanical and thermal thresholds did not differ between genotypes. TTX-resistant current carries the majority of charge during action potentials in nociceptive neurons (3), and TTX-resistant sodium channels have been implicated in pain signaling. In the partial sciatic nerve ligation (Seltzer) model of neuropathic pain, $Na_V1.9-/-$ mice were not different from WT littermates with regard to mechanical hyperalgesia. However, we found that expression of $Na_V1.9$ contributes to the persistent thermal hypersensitivity and spontaneous pain behavior after peripheral administration of inflammatory agents. These data support the notion that inflammatory mediators, including PGE_2 and serotonin, modify the function of $Na_V1.9$ to maintain inflammation-induced hyperalgesia (27).

The biophysical properties of the current carried by $Na_V1.9$ and the contribution of this current to primary afferent excitability have been uncertain. The recent discovery that human embryonic kidney cells cotransfected with recombinant $Na_V1.9$ and the receptor tyrosine kinase TrkB express BDNF-activated currents, similar to those found in hippocampal neurons and SH-SY5Y cells (28) but with properties quite different from those of the persistent current in small-diameter DRG neurons, raised the possibility that the current in DRG neurons is not carried by $Na_V1.9$. Our study confirms the molecular identity of the persistent current as $Na_V1.9$. In contrast to the BDNF-activated current in hippocampal neurons, which was completely blocked by 10 nM saxitoxin but resistant to 50 nM TTX, the persistent current observed in mouse DRG neurons was resistant to both TTX and saxitoxin. Computer simulations suggested that $Na_V1.9$ contributes to setting resting membrane potential and therefore may affect subthreshold depolarization (29). However, we found no differences in passive membrane properties and action potential characteristics between acutely dissociated DRG neurons from WT and $Na_V1.9-/-$ mice.

Fluoride was used as the major intracellular anion for the voltage–clamp recordings reported in this study. Under these conditions, the persistent current is clearly distinguishable from the TTX-resistant current carried by $Na_V1.8$. However, the presence of fluoride may affect some of the biophysical properties of the current. Intracellular fluoride has been reported to cause a hyperpolarizing shift in the voltage dependence of activation and inactivation of the persistent sodium current (30). The use of fluoride in our recordings allowed for unambiguous identification of neurons expressing the persistent sodium current; however, some properties may not be representative of the channel under physiological conditions. The nature of the persistent current under physiological conditions remains unclear. Immediately after achieving the whole-cell conformation, $Na_V1.9$ appears largely silent, in agreement with its lack of contribution to resting membrane potential and action potential characteristics. The increase in persistent current amplitude during whole-cell recording may be the result of cell dialysis, suggestive of a cytoplasmic component that keeps the channel closed under physiological conditions. Alternatively, it could represent the recovery from ultraslow inactivation. Previously, it was estimated that 97% of the persistent current is ultraslow-inactivated at −60 mV (14).

The release of inflammatory mediators after injections of formalin, carrageenan, or CFA sensitizes peripheral nociceptors (31, 32). CFA-induced inflammation increased expression of $Na_V1.9$ mRNA ≈2-fold by day 7 (33), suggesting that altered $Na_V1.9$ expression may contribute to the maintenance of the inflammatory response at this time point. The time course of the formalin response (40 min) is too short to be caused by changes in $Na_V1.9$ expression. Also, carrageenan administration did not increase $Na_V1.9$ mRNA or protein expression (34). Therefore, differences between WT and $Na_V1.9-/-$ mice in their response to formalin- or carrageenan-induced inflammation are likely caused by post-translational modifications of $Na_V1.9$ in the WT animals. PGE_2 has been shown to modulate TTX-R and $Na_V1.9$ currents (18, 27) and may be responsible for maintaining inflammatory hyperalgesia over the time courses studied here, independent of the alogenic substance. The hyperalgesic effects of PGE_2 in primary afferent neurons are mediated by G proteins (35). In DRG neurons, persistent current is increased by GTP and nonhydrolyzable GTP analogs (36), suggesting that $Na_V1.9$ may be modulated by inflammatory mediators, such as 5-hydroxytryptamine, through activation of G proteins. Further, PGE_2-induced changes in Nav1.9 currents were blocked by pertussis toxin, indicating the involvement of G_i and/or G_o.

Together, these results suggest that several sodium channel subtypes contribute differentially to the temporal aspects of pain signaling and that these differences relate, in part, to the mechanisms that underlie peripheral sensitization triggered by inflammatory mediators.

We thank Irene Nunes for critically reading the manuscript and Donghui Zhang and Richard Raubertas for contributions to the statistical analysis of the quantitative PCR data.

1. Kostyuk, P. G., Veselovsky, N. S. & Tsyndrenko, A. Y. (1981) *Neuroscience* **6,** 2423–2430.
2. Elliott, A. A. & Elliott, J. R. (1993) *J. Physiol. (London)* **463,** 39–56.
3. Blair, N. T. & Bean, B. P. (2002) *J. Neurosci.* **22,** 10277–10290.
4. Kral, M. G., Xiong, Z. & Study, R. E. (1999) *Pain* **81,** 15–24.
5. Zhang, X. F., Zhu, C. Z., Thimmapaya, R., Choi, W. S., Honore, P., Scott, V. E., Kroeger, P. E., Sullivan, J. P., Faltynek, C. R., Gopalakrishnan, M. & Shieh, C. C. (2004) *Brain Res.* **1009,** 147–158.
6. Akopian, A. N., Sivilotti, L. & Wood, J. N. (1996) *Nature* **379,** 257–262.
7. Akopian, A. N., Souslova, V., England, S., Okuse, K., Ogata, N., Ure, J., Smith, A., Kerr, B. J., McMahon, S. B., Boyce, S., *et al*. (1999) *Nat. Neurosci.* **2,** 541–548.
8. Renganathan, M., Cummins, T. R. & Waxman, S. G. (2001) *J. Neurophysiol.* **86,** 629–640.
9. Lai, J., Gold, M. S., Kim, C. S., Bian, D., Ossipov, M. H., Hunter, J. C. & Porreca, F. (2002) *Pain* **95,** 143–152.
10. Khasar, S. G., Gold, M. S. & Levine, J. D. (1998) *Neurosci. Lett.* **256,** 17–20.
11. Kerr, B. J., Souslova, V., McMahon, S. B. & Wood, J. N. (2001) *NeuroReport* **12,** 3077–3080.
12. Fang, X., Djouhri, L., Black, J. A., Dib-Hajj, S. D., Waxman, S. G. & Lawson, S. N. (2002) *J. Neurosci.* **22,** 7425–7433.
13. Dib-Hajj, S. D., Tyrrell, L., Black, J. A. & Waxman, S. G. (1998) *Proc. Natl. Acad. Sci. USA* **95,** 8963–8968.
14. Cummins, T. R., Dib-Hajj, S. D., Black, J. A., Akopian, A. N., Wood, J. N. & Waxman, S. G. (1999) *J. Neurosci.* **19,** RC43.
15. Rugiero, F., Mistry, M., Sage, D., Black, J. A., Waxman, S. G., Crest, M., Clerc, N., Delmas, P. & Gola, M. (2003) *J. Neurosci.* **23,** 2715–2725.
16. Fjell, J., Cummins, T. R., Fried, K., Black, J. A. & Waxman, S. G. (1999) *J. Neurophysiol.* **81,** 803–810.
17. Porreca, F., Lai, J., Bian, D., Wegert, S., Ossipov, M. H., Eglen, R. M., Kassotakis, L., Novakovic, S., Rabert, D. K., Sangameswaran, L. & Hunter, J. C. (1999) *Proc. Natl. Acad. Sci. USA* **96,** 7640–7644.
18. Rush, A. M. & Waxman, S. G. (2004) *Brain Res.* **1023,** 264–271.
19. Koerber, H. R. & Woodbury, C. J. (2002) *Physiol. Behav.* **77,** 589–594.
20. Hargreaves, K., Dubner, R., Brown, F., Flores, C. & Joris, J. (1988) *Pain* **32,** 77–88.
21. Chaplan, S. R., Bach, F. W., Pogrel, J. W., Chung, J. M. & Yaksh, T. L. (1994) *J. Neurosci. Methods* **53,** 55–63.
22. Seltzer, Z., Dubner, R. & Shir, Y. (1990) *Pain* **43,** 205–218.
23. Gold, M. S., Shuster, M. J. & Levine, J. D. (1996) *J. Neurophysiol.* **75,** 2629–2646.
24. Scholz, A., Kuboyama, N., Hempelmann, G. & Vogel, W. (1998) *J. Neurophysiol.* **79,** 1746–1754.
25. Nuss, H. B., Tomaselli, G. F. & Marban, E. (1995) *J. Gen. Physiol.* **106,** 1193–1209.
26. Ragsdale, D. S., McPhee, J. C., Scheuer, T. & Catterall, W. A. (1996) *Proc. Natl. Acad. Sci. USA* **93,** 9270–9275.
27. Gold, M. S., Reichling, D. B., Shuster, M. J. & Levine, J. D. (1996) *Proc. Natl. Acad. Sci. USA* **93,** 1108–1112.
28. Blum, R., Kafitz, K. W. & Konnerth, A. (2002) *Nature* **419,** 687–693.
29. Herzog, R. I., Cummins, T. R. & Waxman, S. G. (2001) *J. Neurophysiol.* **86,** 1351–1364.
30. Coste, B., Osorio, N., Padilla, F., Crest, M. & Delmas, P. (2004) *Mol. Cell. Neurosci.* **26,** 123–134.
31. Dirig, D. M., Isakson, P. C. & Yaksh, T. L. (1998) *J. Pharmacol. Exp. Ther.* **285,** 1031–1038.
32. Damas, J. & Liegeois, J. F. (1999) *Naunyn-Schmiedeberg's Arch. Pharmacol.* **359,** 220–227.
33. Tate, S., Benn, S., Hick, C., Trezise, D., John, V., Mannion, R. J., Costigan, M., Plumpton, C., Grose, D., Gladwell, Z., *et al*. (1998) *Nat. Neurosci.* **1,** 653–655.
34. Black, J. A., Liu, S., Tanaka, M., Cummins, T. R. & Waxman, S. G. (2004) *Pain* **108,** 237–247.
35. Taiwo, Y. O. & Levine, J. D. (1989) *Brain Res.* **492,** 400–403.
36. Baker, M. D., Chandra, S. Y., Ding, Y., Waxman, S. G. & Wood, J. N. (2003) *J. Physiol. (London)* **548,** 373–382.